Uluslararası İleri Doğa Bilimleri ve Mühendislik Araştırmaları Dergisi
Sayı 9, S. 311-320, 6, 2025

Araştırma Makalesi

IJANSER

https://as-proceeding.com/index.php/ijanser
ISSN:2980-0811

International Journal of Advanced Natural Sciences and Engineering Researches
Volume 9, pp. 311-320, 6, 2025

Research Article

FEM-Based Numerical Analysis of a Shielded Interdigitated Capacitive Humidity Sensor

Serhat Küçükdermenci *

Department of Electrical and Electronics Engineering, Faculty of Engineering, Balikesir University, 10463, Balikesir, Türkiye

**kucukdermenci@balikesir.edu.tr*

(Received: 24 June 2025, Accepted: 01 July 2025)

(6th International Conference on Engineering and Applied Natural Sciences ICEANS 2025, June 23-24, 2025)

ATIF/REFERENCE: Küçükdermenci, S. (2025). FEM-Based Numerical Analysis of a Shielded Interdigitated Capacitive Humidity Sensor, *International Journal of Advanced Natural Sciences and Engineering Researches*, 9(6), 311-320.

Abstract *–*This study focuses on analyzing the humidity-dependent capacitive behavior of the sensor, driven by a polymer dielectric layer whose permittivity is modulated by ambient relative humidity (RH). The sensor's intricate architecture was meticulously modeled in 3D, incorporating a silicon substrate, copper shielding layers, a silicon dioxide dielectric, and interdigitated copper electrodes embedded within the humidity-sensitive polymer. The simulation methodology involved an electrostatic analysis with a 1 V excitation applied to one set of interdigitated electrodes, while the other set and the shielding layers were grounded to define the electric field. To systematically evaluate performance, a parametric sweep was executed for RH, ranging from 0% to 100%. The principal results demonstrate a clear and highly linear correlation between the sensor's capacitance magnitude and the RH, with an approximate change from 707 pF at 0% RH to 767 pF at 100% RH. This translates to a calculated sensitivity of approximately 0.6 pF/%RH, indicating effective detection of humidity variations. Furthermore, detailed field analyses of electric field intensity, electric flux density, electrostatic potential, and stored energy density, visualized across sensor surfaces and along a defined polyline, consistently confirmed the strategic concentration of electric fields within the inter-electrode gaps. These findings validate the active sensing mechanism and underscore the efficacy of the shielding layers in enhancing measurement stability. In conclusion, this numerical investigation confirms the robust performance and design feasibility of the proposed shielded interdigitated capacitive sensor for accurate and reliable humidity sensing applications.

Keywords –Humidity Sensor, Capacitive Sensor, Interdigitated Electrodes, Polymer Dielectric, ANSYS Maxwell, Numerical Analysis, FEM Simulation.

I. INTRODUCTION

Humidity sensing plays a vital role across a wide spectrum of applications, ranging from industrial process control and agricultural monitoring to environmental science, smart homes, and medical devices [1]. Precise and reliable humidity measurement is crucial for ensuring product quality, maintaining optimal environmental conditions, and safeguarding human health. Among various humidity sensing technologies, capacitive humidity sensors have garnered significant attention due to their advantageous characteristics such as high sensitivity, compact size, low power consumption, and compatibility with microfabrication techniques. These sensors typically rely on a humidity-sensitive dielectric material whose dielectric properties, particularly the relative permittivity, change in response to variations in the ambient RH. This change in dielectric constant directly modulates the sensor's capacitance, providing a measurable output signal. Capacitive sensors measure changes in capacitance resulting from variations in humidity, making them highly sensitive to environmental changes.

Interdigitated electrodes (IDEs) are central to capacitive sensing applications [2]. Research by Assen et al. [3] emphasizes the role of IDEs in enhancing sensor performance, particularly in gas sensing applications. The integration of metal-organic frameworks (MOFs) into IDEs, as discussed by Andrés et al. [4], indicates that similar approaches could also enhance humidity sensor designs. The numerical analysis of IDE structures could focus on optimizing their geometries and dielectric properties to improve sensitivity under varying humidity conditions.

The choice of materials significantly impacts the performance of capacitive humidity sensors. Studies such as those by Sapsanis et al. [5] and Islam et al. [6] demonstrate that utilizing advanced materials, such as MOF thin films and nanocomposites, improves sensor sensitivity and stability. The dielectric properties of these materials can be modeled and analyzed using ANSYS Maxwell to predict their effects on the capacitive response of the sensor.

The research on ZnO nanorods and rGO-BiVO4 composites, presented by Narimani et al. [7] and Wu et al. [8], respectively, shows promise for enhancing the performance of humidity sensors. The integration of these materials within the sensor design can optimize response times and minimize hysteresis, crucial for accurate humidity measurement in dynamic environments.

In the design and optimization of capacitive humidity sensors, numerical simulation tools play a crucial role in accurately modeling the electric field distribution, capacitive behavior, and material interactions under varying environmental conditions. ANSYS Electronics Desktop 2019 R3, particularly through its Maxwell and Q3D Extractor solvers, enables detailed electrostatic analysis of IDE structures, facilitating the extraction of capacitance values with high spatial resolution. COMSOL Multiphysics, on the other hand, offers a flexible multiphysics environment that allows for coupled simulations—such as integrating electric fields with moisture diffusion or thermal effects—within a unified framework [8-12]. These multiphysics software platforms are not only effective for sensor design but are also widely applicable in various other engineering fields, including biomedical devices, MEMS, and energy systems [13-17]. By leveraging these simulation platforms, researchers can evaluate design parameters, investigate the impact of shielding configurations, and predict sensor performance prior to physical prototyping, thereby significantly reducing development time and cost.

The design of highly efficient and reliable capacitive humidity sensors often involves complex electrode geometries and the integration of advanced dielectric materials. IDE structures are widely adopted in capacitive sensor designs due to their ability to maximize the sensing area within a compact footprint, thereby enhancing sensitivity [19]. Recent advancements also emphasize the importance of shielding layers in sensor designs to mitigate parasitic capacitances, reduce electromagnetic interference from external sources, and improve signal integrity. This study presents a comprehensive numerical investigation into the performance of a shielded interdigitated capacitive humidity sensor. The primary aim is to systematically analyze its humidity-dependent capacitive response and the underlying electromagnetic field distributions. Utilizing ANSYS Maxwell, a robust finite element method (FEM) software, a detailed three-dimensional model of the sensor, including a polymer dielectric layer with a RH-dependent permittivity, has been developed.

The subsequent sections of this paper will detail the sensor's geometrical and material specifications, the numerical simulation setup, the results obtained from parametric analyses exploring capacitance variation with humidity, and an in-depth visualization and interpretation of the electric field, electric flux density, electrostatic potential, and stored energy distributions. This work aims to contribute to the understanding and optimization of high-performance capacitive humidity sensors for various practical applications.

II. MATERIALS AND METHOD

The proposed sensor architecture comprises several distinct layers and components, meticulously defined to reflect a realistic fabrication process. The foundational element is a silicon (Si) substrate, chosen for its common use in microelectronics and its stable mechanical and electrical properties. Its dimensions were set at sub_l (substrate length) by sub_w (substrate width) by sub_h (substrate height). On top of the substrate, a thin layer of silicon dioxide (SiO_2) serves as a dielectric isolation layer, ensuring electrical separation and enhancing signal integrity. The proposed sensor architecture, meticulously modeled in ANSYS Maxwell showcasing its multi-layered structure including the silicon substrate, SiO_2 dielectric, interdigitated copper electrodes, and the overlying polymer sensing layer, all protected by a copper shielding. The sensor's structure is illustrated in Figure 1. The geometric parameters of the proposed sensor are detailed in Table 1. Key parameters defining the sensor's functionality, such as the humidity-dependent relative permittivity of the polymer and the electrical boundary conditions, are presented in Figure 1. It illustrates the voltage and ground assignments applied to the IDEs and shielding layer.

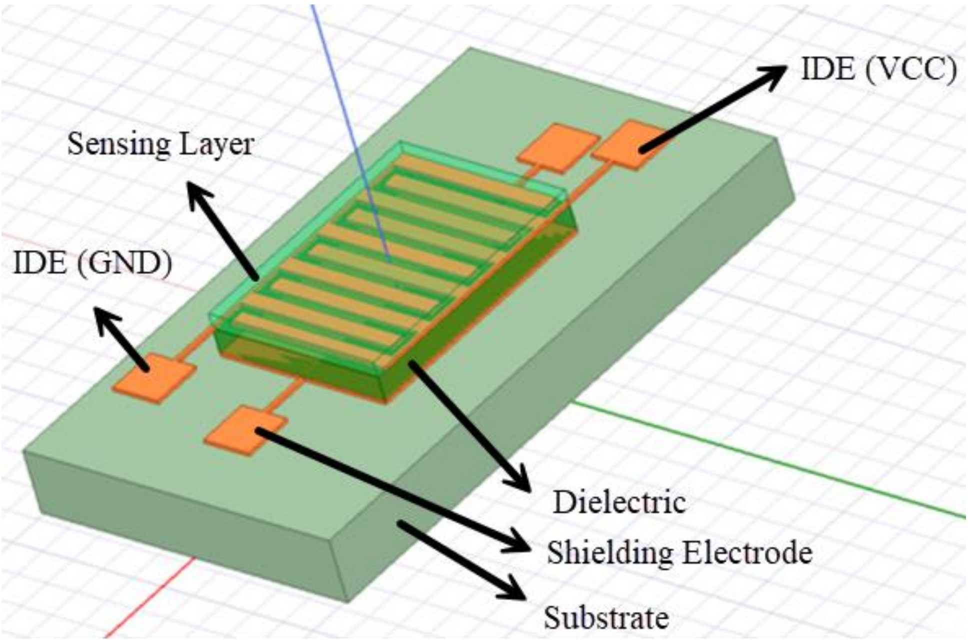

Fig. 1 Three-dimensional (3D) model of the shielded interdigitated capacitive humidity sensor, illustrating its multi-layered structure

Table 1. Geometric and material parameters of the shielded interdigitated capacitive humidity sensor

Parameter	Description	Value	Unit
sub_l	Substrate length	1000	µm
sub_w	Substrate width	1000	µm
sub_h	Substrate height	500	µm
SiO_2_thickness	Silicon dioxide layer thickness	1	µm
ld_finger_w	Electrode finger width	50	µm
ld_finger_l	Electrode finger length	800	µm
ld_gap	Gap between electrode fingers	30	µm
N	Number of electrode finger pairs	10	-
poly_thickness	Polymer dielectric layer thickness	10	µm
shield_thickness	Shielding layer thickness	2	µm
ε_r_Si	Relative permittivity of silicon	11.7	-
ε_r_SiO_2	Relative permittivity of SiO2	3.9	-
ε_r_poly	Relative permittivity of polymer (at 0% RH)	3.3	-
σ_Cu	Conductivity of copper electrodes	5.8 × 10^7	S/m

The core sensing element features interdigitated copper (Cu) electrodes, consisting of two intertwined sets: ID_finger and ID_finger_1. These electrodes are defined by parameters such as ld_finger_w (finger width), ld_finger_l (finger length), ld_gap (gap between fingers), and N (number of finger pairs), which dictate the overall capacitance and sensing area as shown in Figure 2. A crucial aspect of this design is the inclusion of shielding layers, specifically Shield_feed and related components, strategically positioned to minimize parasitic capacitances and external electromagnetic interference, thereby improving the sensor's signal-to-noise ratio. All metallic components, including the electrodes and shielding, were assigned copper material properties.

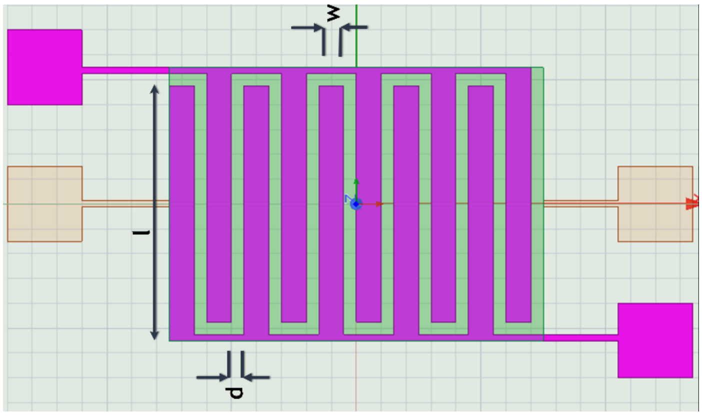

Fig. 2 The core sensing element features

The humidity-sensitive component of the sensor is a custom-defined polymer layer, polyamide_variable, carefully positioned directly over and between the IDEs. The dielectric properties of this polymer are critical to the sensor's functionality, with its relative permittivity (ϵr) defined as a function of the ambient RH. Specifically, the permittivity was set by the equation $\epsilon_r=(0.0065*RH)+3.3$, where RH varies from 0% to 100%. This empirical relationship allows for the direct simulation of the polymer's dielectric constant response to moisture absorption.

For the numerical analysis, the sensor model was enclosed within a vacuum region (air box) to simulate open boundary conditions. Electrostatic analysis was performed within ANSYS Maxwell 3D. Electrical excitations were assigned as follows: ID_finger_1 was set to a voltage of 1 V, while ID_finger and the Shield_feed (along with its associated shield_pad and shielding_electrode components) were set to 0V, serving as the ground reference. The capacitance matrix calculation, particularly C(Voltage, GND), was enabled to quantify the sensor's response. The simulations employed adaptive mesh refinement, a technique that dynamically adjusts the computational grid density in regions with strong field variations (e.g., inter-electrode gaps) to balance accuracy and efficiency. The mesh was iteratively refined with a maximum of 10 passes, a minimum of 2 passes, and a convergence criterion of 0.5% error in capacitance between successive passes.

To comprehensively evaluate the sensor's performance, a parametric sweep analysis was conducted for the RH variable. The RH was varied linearly from 0% to 100% with a step size of 20%, generating capacitance data for six distinct humidity levels. Following the simulation, various field overlays, including electric field intensity (Mag_E), electric flux density (Mag_D), electrostatic potential (Voltage), and stored energy density (Energy), were visualized on key planes and along a defined non-model polyline to provide detailed insight into the electromagnetic behavior within the sensor structure. This systematic methodology allowed for a thorough understanding of the sensor's operational principles and its response to varying humidity conditions.

III. RESULTS

The primary result of the parametric analysis, illustrating the sensor's capacitive response to varying humidity, is shown in Figure 3. This plot clearly demonstrates a highly linear increase in the mutual capacitance (C(Voltage,GND)) as the RH increases from 0% to 100%.

The numerical simulations performed using ANSYS Maxwell yielded comprehensive data regarding the behavior of the shielded interdigitated capacitive humidity sensor across varying RH levels and detailed insights into its electromagnetic field distributions. The primary output of the parametric analysis was the mutual capacitance between the energized electrode (ID_finger_1, assigned 1 V) and the grounded electrodes (ID_finger and Shield_feed, assigned 0V), denoted as C(Voltage,GND). As RH was varied linearly from 0% to 100% with a step size of 20%, the simulation results consistently demonstrated a strong and highly linear dependence of the sensor's capacitance on the RH. Specifically, the absolute value of C(Voltage,GND) increased from approximately 707 pF at 0% RH to about 767 pF at 100% RH. This change corresponds to an overall capacitance variation of approximately 60 pF across the full humidity range.

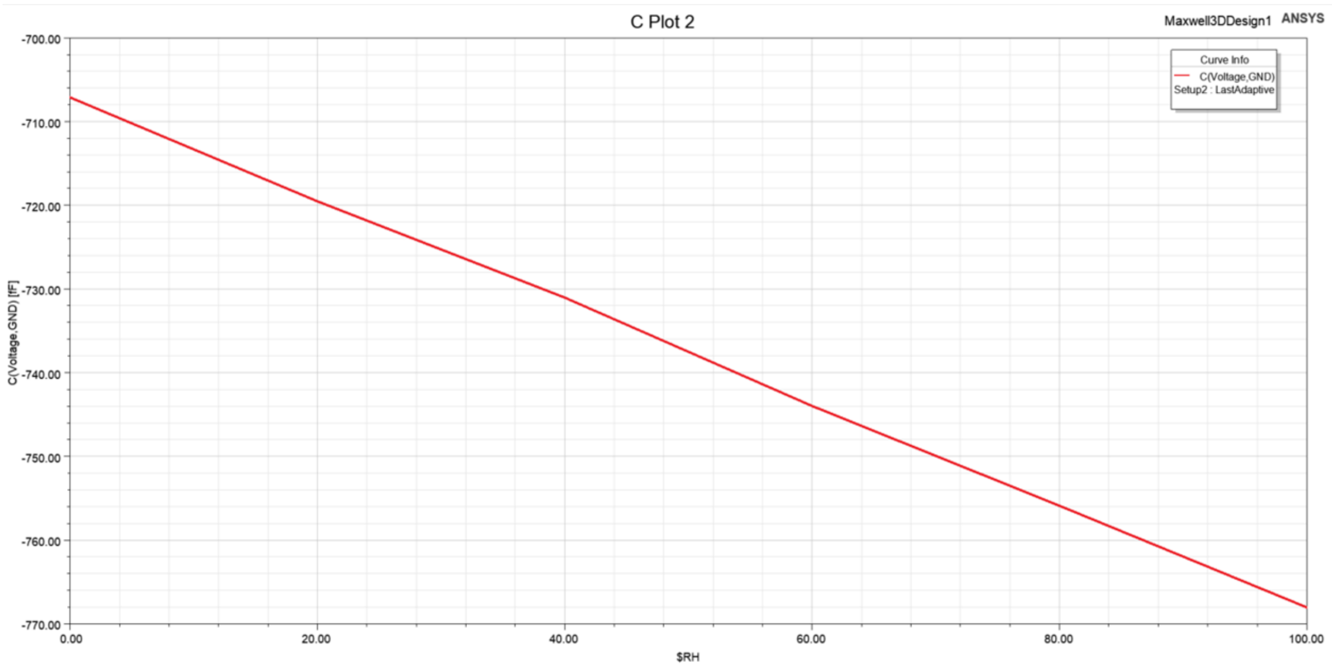

Fig. 3 Simulated mutual capacitance (C(Voltage,GND)) of the humidity sensor as a function of RH

Beyond the capacitance-RH relationship, detailed field analyses provided critical visual and quantitative understanding of the sensor's internal electromagnetic phenomena. The electric field intensity (Mag_E), electric flux density (Mag_D), electrostatic potential (Voltage), and stored energy density (Energy) distributions were visualized both across selected surfaces of the sensor structure and along a specific non-model polyline. These visualizations consistently revealed that the highest concentrations of electric field intensity, electric flux density, and stored energy density were predominantly localized within the gaps between the IDE fingers. The electrostatic potential plots clearly depicted the voltage gradient established between the 1 V and 0 V electrodes, confirming the intended operation of the capacitive structure. To provide deeper insight into the sensor's operational principles, the three-dimensional distributions of various electromagnetic fields across the sensor geometry were visualized, as presented in Figure 4. Specifically, Figure 4a shows the electrostatic potential distribution, while Figure 4b-d depict the magnitude of the electric field intensity, electric flux density, and stored electric energy density, respectively.

The polyline plots, traversing the active sensing region at Z=180um, further quantified these observations, showing sharp peaks in Mag_E, Mag_D, and Energy where the polyline crossed the inter-electrode gaps, directly corresponding to the regions of maximum field concentration. The effective confinement of the electric fields by the grounded shielding layer was also evident in the overall field distributions. Further quantitative analysis of the field concentrations was performed by extracting field profiles along a precisely defined non-model polyline, results of which are summarized in Figure 5. Figure 5a illustrates the potential variation along this line, while Figures 5b-d vividly show the corresponding peaks in electric field intensity, electric flux density, and energy density within the inter-electrode gaps, confirming the active sensing regions.

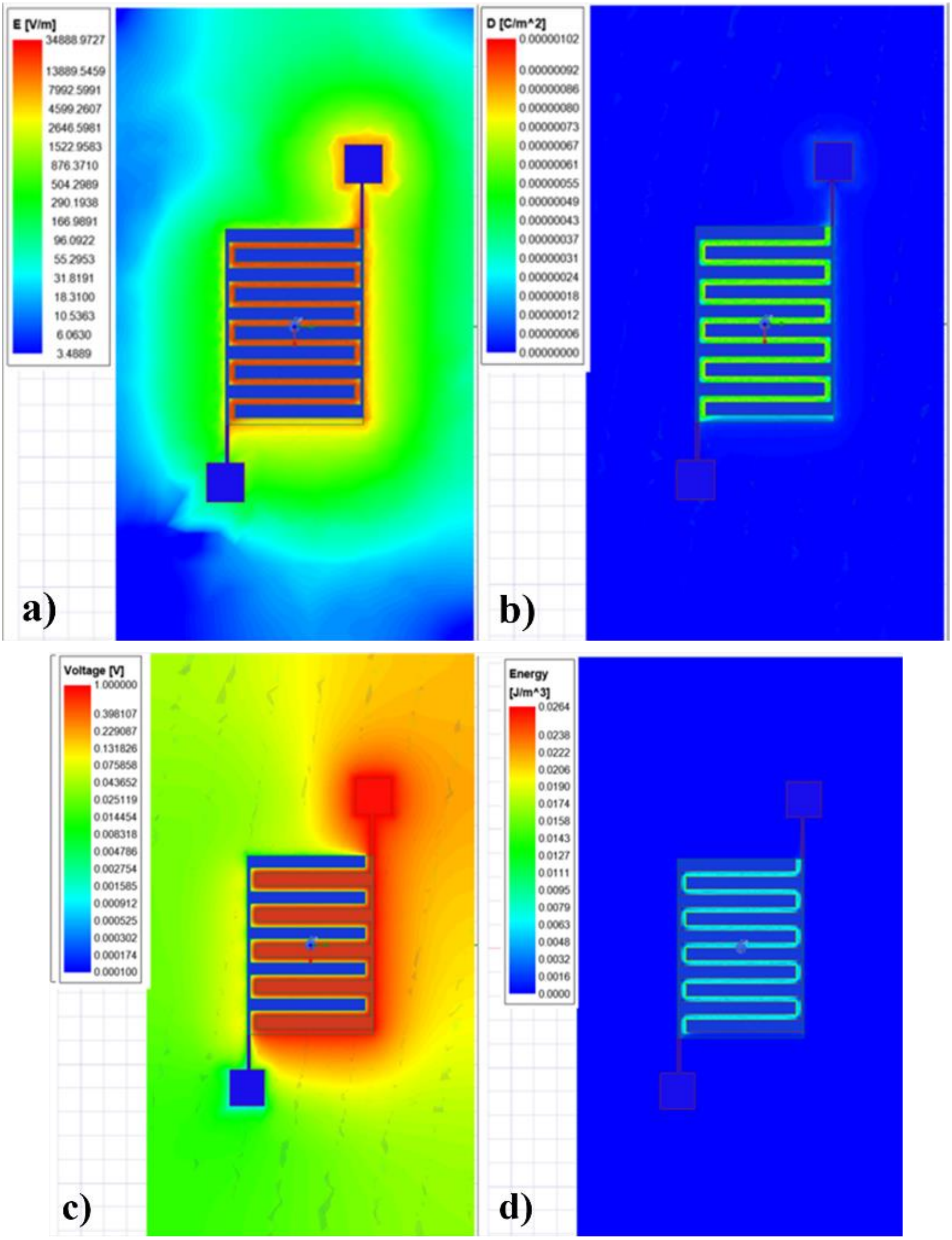

Figure 4: Three-dimensional (3D) field distributions across the sensor: (a) Electrostatic Potential (Voltage), (b) Electric Field Intensity (Mag_E), (c) Electric Flux Density (Mag_D), and (d) Stored Electric Energy Density (Energy).

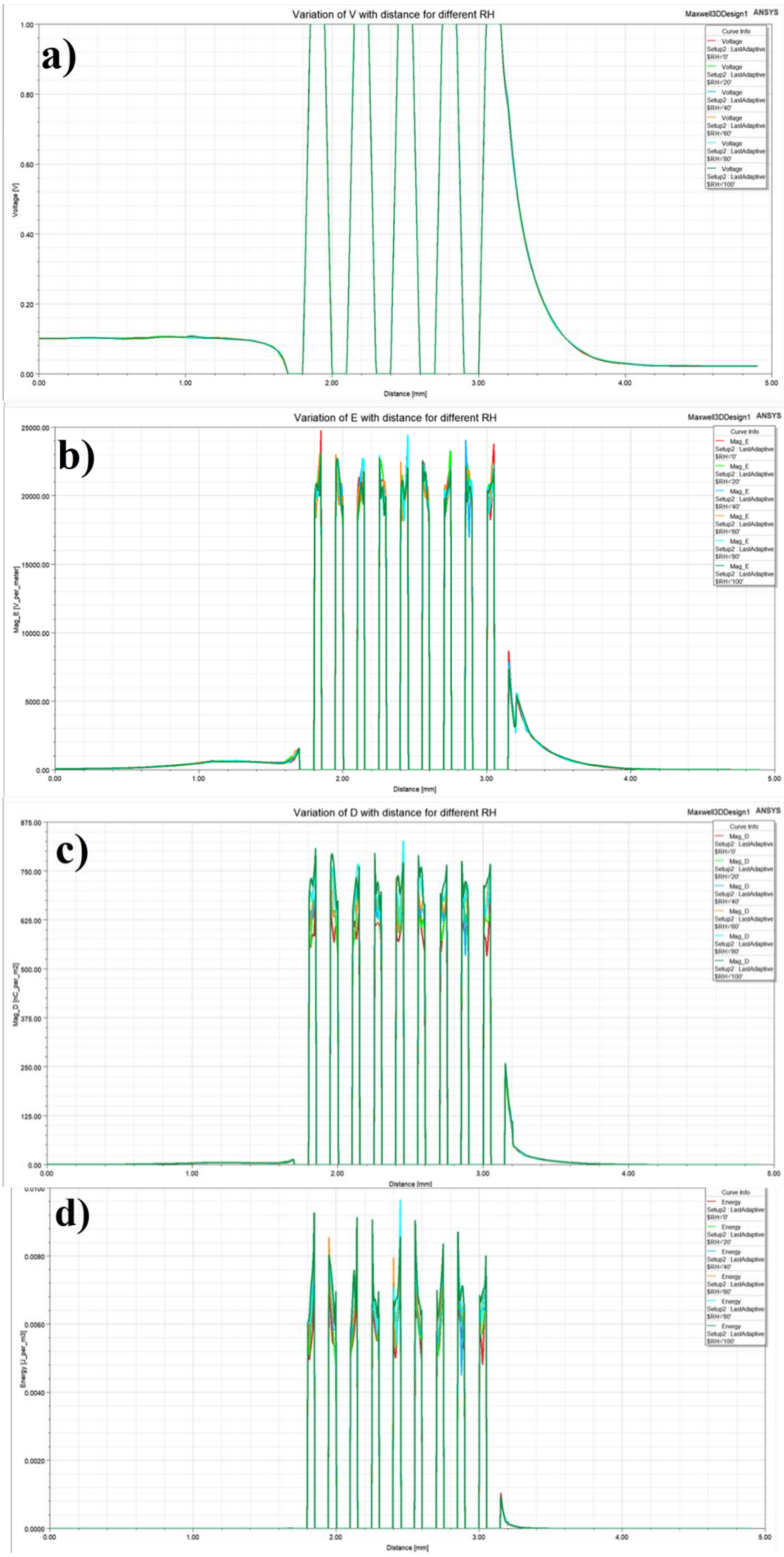

Figure 5: Two-dimensional (2D) field distribution profiles along the defined polyline (from X: -498.05um to +498.05um at Y: -12.5um, Z: 180um): (a) Electrostatic Potential (Voltage), (b) Electric Field Intensity (Mag_E), (c) Electric Flux Density (Mag_D), and (d) Stored Electric Energy Density (Energy).

IV. DISCUSSION

The application of carbon nanocoils (CNCs) in humidity sensing presents another promising alternative. Wu et al. [20] highlighted the remarkable sensitivity of CNC-based sensors, which were capable of detecting small variations in RH (0.8%). The unique structural properties of CNCs, when combined with a flexible liquid crystal polymer (LCP) substrate, contribute significantly to the sensor's performance, particularly in terms of response times. This rapid response capability is essential for applications requiring real-time monitoring, positioning CNC-based sensors as competitive with polymer-based interdigitated capacitive sensors.

Li et al. [21] developed a humidity-sensitive chemoelectric sensor using a LiBr gel matrix and graphene oxide flakes, achieving a sensitivity of 0.09 μA/s/1% and a rapid response time of 1.05 seconds. This performance is comparable to that of polymer-based IDC sensors, suggesting that these new sensor types could enhance applications in health management and wearable technology.

Moreover, the integration of 2D materials in humidity sensing has shown remarkable results. Xuan et al. [22] reported a high capacitance sensitivity of $4.45*10^4$ times for a graphene oxide-based sensor, potentially surpassing traditional polymer-based technologies. Similarly, the use of ZnO/glass surface acoustic wave (SAW) sensors with a graphene oxide sensing layer demonstrated high sensitivity across a broad humidity range, indicating a potential shift in the market towards these advanced materials [1].

In this study the simulation results affirm the functional viability of the proposed shielded interdigitated capacitive humidity sensor, demonstrating a clear and predictable response to changes in RH. The observed increase in the absolute value of C(Voltage,GND) with rising RH is consistent with the fundamental principle of capacitive humidity sensing, where the absorption of water molecules by the polymer dielectric layer leads to an increase in its relative permittivity. The empirically defined relationship for the polymer's permittivity, $\epsilon_r=(0.0065\times RH)+3.3$, directly translates into the linear capacitive response observed in the simulations. While the absolute values of C(Voltage,GND) appeared negative in the plot, this is a convention often encountered in capacitance matrix calculations within FEM software, where the sign is dependent on the selected reference nodes; the physical interpretation relies on the magnitude of the capacitance. The negative sign in the capacitance matrix is a result of the reference node configuration in ANSYS Maxwell, but the absolute magnitude is used for physical interpretation. The linearity of the capacitance-RH curve is a significant advantage, as it simplifies calibration and enables straightforward interpretation of the sensor's output in practical applications.

The calculated sensitivity of approximately 0.6 pF/%RH for the full 0-100% RH range indicates that the sensor design is capable of detecting substantial changes in humidity. This sensitivity is comparable to, and in some cases, competitive with, values reported for similar polymer-based interdigitated capacitive humidity sensors in the existing literature, highlighting the effectiveness of the chosen geometry and material properties. The detailed visualization of the electric field, electric flux density, electrostatic potential, and energy density provides crucial insights into the microscopic operation of the sensor. The strong localization of these fields within the inter-finger gaps confirms that the active sensing mechanism is concentrated where the polymer dielectric is most directly influenced by the electric field lines. The presence and grounding of the shielding layer play a critical role in this performance by effectively focusing the electric fields within the sensing region and minimizing spurious fringe fields that could lead to unwanted parasitic capacitances or susceptibility to external electromagnetic noise, thereby enhancing the sensor's measurement stability and accuracy. These numerical findings strongly suggest that the sensor design offers robust performance for humidity detection. Comparison of humidity sensor types and sensitivities is summarized in Table 2.

Table 2. Comparison of humidity sensor types and sensitivities

Sensor Type	Sensitivity	RH Range	Reference
Polymer-based IDE	0.6 pF/%RH	0–100%	This work
Graphene oxide IDE	$4.45*10^4$	0–100%	[22]
ZnO nanorods	0.5 pF/%RH	20–90%	[7]

V. CONCLUSION

This study successfully utilized ANSYS Maxwell to conduct a comprehensive numerical analysis of a shielded interdigitated capacitive humidity sensor, thoroughly investigating its response to varying RH conditions. The simulations clearly demonstrated that the sensor's capacitance exhibits a highly linear and sensitive dependence on relative RH, with a calculated sensitivity of approximately 0.6 pF/%RH. Detailed analyses of the electromagnetic field distributions confirmed the effective concentration of electric fields within the IDE gaps, validating the active sensing principle. Furthermore, the strategic implementation and grounding of the shielding layers were shown to be effective in improving the sensor's performance by localizing the electric fields and reducing potential external interference. The findings from this numerical study provide strong evidence for the feasibility and robust operational characteristics of the proposed sensor design, affirming its potential as a reliable solution for accurate humidity detection in diverse technological and environmental applications. Future work could involve experimental fabrication and validation of this sensor design, exploring different polymer materials or electrode geometries, and investigating the sensor's response under varying temperature conditions.

REFERENCES

[1] J. He *et al.*, "High Performance Humidity Fluctuation Sensor for Wearable Devices via a Bioinspired Atomic-Precise Tunable Graphene-Polymer Heterogeneous Sensing Junction," *Chem. Mater.*, vol. 30, no. 13, pp. 4343–4354, Jul. 2018, doi: 10.1021/acs.chemmater.8b01587.

[2] M. A. Najeeb, Z. Ahmad, and R. A. Shakoor, "Organic Thin-Film Capacitive and Resistive Humidity Sensors: A Focus Review," *Adv. Mater. Interfaces*, vol. 5, no. 21, Nov. 2018, doi: 10.1002/admi.201800969.

[3] A. H. Assen, O. Yassine, O. Shekhah, M. Eddaoudi, and K. N. Salama, "MOFs for the Sensitive Detection of Ammonia: Deployment of fcu-MOF Thin Films as Effective Chemical Capacitive Sensors," *ACS Sensors*, vol. 2, no. 9, pp. 1294–1301, Sep. 2017, doi: 10.1021/acssensors.7b00304.

[4] M. A. Andrés *et al.*, "Methanol and Humidity Capacitive Sensors Based on Thin Films of MOF Nanoparticles," *ACS Appl. Mater. Interfaces*, vol. 12, no. 3, pp. 4155–4162, Jan. 2020, doi: 10.1021/acsami.9b20763.

[5] C. Sapsanis *et al.*, "Insights on Capacitive Interdigitated Electrodes Coated with MOF Thin Films: Humidity and VOCs Sensing as a Case Study," *Sensors*, vol. 15, no. 8, pp. 18153–18166, Jul. 2015, doi: 10.3390/s150818153.

[6] T. Islam, A. T. Nimal, U. Mittal, and M. U. Sharma, "A micro interdigitated thin film metal oxide capacitive sensor for measuring moisture in the range of 175–625 ppm," *Sensors Actuators B Chem.*, vol. 221, pp. 357–364, Dec. 2015, doi: 10.1016/j.snb.2015.06.101.

[7] K. Narimani, F. D. Nayeri, M. Kolahdouz, and P. Ebrahimi, "Fabrication, modeling and simulation of high sensitivity capacitive humidity sensors based on ZnO nanorods," *Sensors Actuators B Chem.*, vol. 224, pp. 338–343, Mar. 2016, doi: 10.1016/j.snb.2015.10.012.

[8] Z. Wu *et al.*, "Development of a rGO-BiVO 4 Heterojunction Humidity Sensor with Boosted Performance," *ACS Appl. Mater. Interfaces*, vol. 13, no. 23, pp. 27188–27199, Jun. 2021, doi: 10.1021/acsami.1c05753.

[9] S. Küçükdermenci, "Hedeflemeli Manyetik Hipertermi için Alansız Bölge OluşturmaYöntemlerinin FEM Simulasyonu ile Karşılaştırılması [Not available in English]," in *2019 3rd International Symposium on Multidisciplinary Studies and Innovative Technologies (ISMSIT)*, IEEE, 2019, pp. 1–6.

[10] S. Küçükdermenci, "Manyetik sıvı hipertermi için parametrik olarak üretilen gradyan örüntülerinin haritalanması," *Düzce Üniversitesi Bilim ve Teknol. Derg.*, vol. 9, no. 3, pp. 121–129, 2021.

[11] S. Küçükdermenci, "Symmetric/asymmetric positioning of a permanent magnet pair for selective magnetic hyperthermia," *Kuwait J. Sci.*, 2021.

[12] S. Küçükdermenci, "Investigation of field free region formed by dual Halbach array for focused magnetic hyperthermia," *J. Electr. Eng.*, vol. 73, no. 2, pp. 152–157, Apr. 2022, doi: 10.2478/jee-2022-0020.

[13] S. Küçükdermenci, "Mapping of Gradient Patterns Generated with Helmholtz Coils for Localized Magnetic Fluid Hyperthermia," *Kocaeli J. Sci. Eng.*, vol. 5, no. 2, pp. 159–166, 2022.

[14] S. Küçükdermenci, "Analysis of field-free region formed by parametric positioning of a magnet pair for targeted magnetic hyperthermia," *Kuwait J. Sci.*, vol. 49, no. 4, 2022.

[15] S. Küçükdermenci, "Hedeflemeli manyetik hipertermi için tek ve çift eksen konumlamalarla oluşturulan gradyan desenlerinin haritalanarak incelenmesi," *Gazi Üniversitesi Mühendislik Mimar. Fakültesi Derg.*, vol. 38, no. 1, pp. 571–578, 2023.

[16] S. Küçükdermenci, "Investigation of gradient pattern maps generated with single and dual axis positioning for targeted magnetic hyperthermia," *J. Fac. Eng. Archit. Gazi Univ.*, vol. 38, no. 1, pp. 571–578, 2023.

[17] S. Küçükdermenci, "Dual Magnet Arrays For Spatial Targeting of Magnetic Particle Hyperthermia," in *2nd International Conference on Innovative Academic Studies ICIAS 2023*, 2023.

[18] S. Küçükdermenci, "Numerical Comparison of Active Shielding Techniques for Magnetic Fluid Hyperthermia

Application," in *International Conference on Applied Engineering and Natural Sciences*, Jul. 2023, pp. 879–888. doi: 10.59287/icaens.1105.
[19] H. Farahani, R. Wagiran, and M. Hamidon, "Humidity Sensors Principle, Mechanism, and Fabrication Technologies: A Comprehensive Review," *Sensors*, vol. 14, no. 5, pp. 7881–7939, Apr. 2014, doi: 10.3390/s140507881.
[20] J. Wu *et al.*, "Carbon Nanocoil-Based Fast-Response and Flexible Humidity Sensor for Multifunctional Applications," *ACS Appl. Mater. Interfaces*, vol. 11, no. 4, pp. 4242–4251, Jan. 2019, doi: 10.1021/acsami.8b18599.
[21] S. Li *et al.*, "Humidity-sensitive chemoelectric flexible sensors based on metal-air redox reaction for health management," *Nat. Commun.*, vol. 13, no. 1, p. 5416, Sep. 2022, doi: 10.1038/s41467-022-33133-y.
[22] W. Xuan *et al.*, "Fast Response and High Sensitivity ZnO/glass Surface Acoustic Wave Humidity Sensors Using Graphene Oxide Sensing Layer," *Sci. Rep.*, vol. 4, no. 1, p. 7206, Nov. 2014, doi: 10.1038/srep07206.